

Ultimate torsional behaviour of axially restrained RC beams

Luís F.A. Bernardo^{*}, Cátia S.B. Taborda^a and Jorge M.A. Andrade^b

Department of Civil Engineering and Architecture, Centre of Materials and Building Technologies (C-made), University of Beira Interior, Covilhã, Portugal

(Received December 12, 2012, Revised June 15, 2015, Accepted July 7, 2015)

Abstract. This article presents a computing procedure developed to predict the torsional strength of axially restrained reinforced concrete beams. This computing procedure is based on a modification of the Variable Angle Truss Model to account for the influence of the longitudinal compressive stress state due to the axial restraint conditions provided by the connections of the beams to other structural elements. Theoretical predictions from the proposed model are compared with some experimental results available in the literature and also with some numerical results from a three-dimensional nonlinear finite element analysis. It is shown that the proposed computing procedure gives reliable predictions for the ultimate behaviour, namely the torsional strength, of axially restrained reinforced concrete beams under torsion.

Keywords: reinforced concrete; beams; torsion; axial restraint; truss-model; finite element analysis

1. Introduction

In current structural procedures, the design of common Reinforced Concrete (RC) beams is usually carried out neglecting the effect of the axial restraint provided by the connections to other structural elements (beams, columns, walls, etc.) which composes the structure in which the beams are inserted (Fig. 1). If the loading and the associated internal stress state of the beam induces an axial positive deformation (elongation), then an additional longitudinal compressive stress state due to the axial restraint will be generated. The magnitude of this stress state will depend on the loading level of the beam (related with the behavioral stage) and also on the level of the axial restraint provided by the stiffness of the connections to the other structural elements.

Experimental results show that, in cracked stage, RC beams under torsion suffer a notable longitudinal elongation (for instance: Hsu 1968 for plain beams, Bernardo and Lopes (2009) for hollow beams). Such longitudinal elongation increases until maximum torque is reached. Then, if beams are axially restrained it is expected that a variable longitudinal compressive stress state will act in addition to the pure shear stress state due to torsion.

It is known that shear strength of RC beams increases due to the influence of a simultaneous and longitudinal compressive stress state. Current codes of practice (for instance, Eurocode 2 2010)

^{*} Corresponding author, Assistant professor, E-mail: lfb@ubi.pt

^a Master, E-mail: tabordacatia@gmail.com

^b Assistant Professor, E-mail: jandrade@ubi.pt

usually provide clauses in order to account for such favorable effect when calculating shear strength. Therefore it is expected that torsional strength of RC beams also increases due to the influence of longitudinal compressive stress states, since high shear stresses also exist. So far, current codes of practice don't include clauses in order to account for this favorable effect when calculating the torsional strength.

Since the original Space-Truss Analogy (STA) proposed in the beginning of last century by Rausch (1929), several further versions have been developed to lead to theoretical models for RC beams under torsion. The STA as a high historical value and constitutes the base for torsion design of the European Model Code (since 1978) and also the American Code (since 1995). One of the STA developments most used in research is the Variable Angle Truss-Model (VATM) (Hsu and Mo 1985a). This theory uses a nonlinear softened stress (σ) – strain (ε) relationship for the concrete in the struts instead of a conventional σ - ε relationship for uniaxial compression. VATM is able to predict the global behaviour of RC beams under torsion throughout the entire loading history, although very good results are observed only for high loading levels (Bernardo *et al.* 2012a). For such levels of loading, the concrete is extensively cracked, so in this stage the theoretical model approaches the real model.

VATM was already extended to Prestressed Concrete (PC) beams under torsion (with longitudinal centered prestress) (Hsu and Mo 1985b). Recently VATM was also modified to predict the global behaviour of RC beams under torsion, including for low loading levels (Bernardo *et al.* 2012b).

Other recent and alternative theoretical models were proposed by several authors in order to compute the torsional strength of RC and PC beams (for instance, Jeng and Hsu 2009, Jeng *et al.* 2010, Cevik *et al.* 2012). However, the mathematical treatment of such models is somehow complex for practical use and they hardly provide a simple concept of how a RC or PC beam behaves under torsion after cracking. VATM is recognized as a model which provides a simple physical understanding of the torsion phenomenon in RC and PC beams.

If rationally applied, longitudinal prestress increases the resistance to cracking of a RC element subject to shear or torsion. In fact, prestress induces a compressive stress which, in combination with the shear stress induced by shear or torsional moment, results in a biaxial stress state (shear + compression). This biaxial stress state delays the cracking of the concrete. Furthermore, since the tensile strength of concrete don't increase in the same proportion as compressive strength increase, it is not possible to reach the full potential of concrete in structures in which resistance is governed by tensile stresses, such as those induced by shear or torsion forces. Therefore, prestress can also increase the torsional strength.

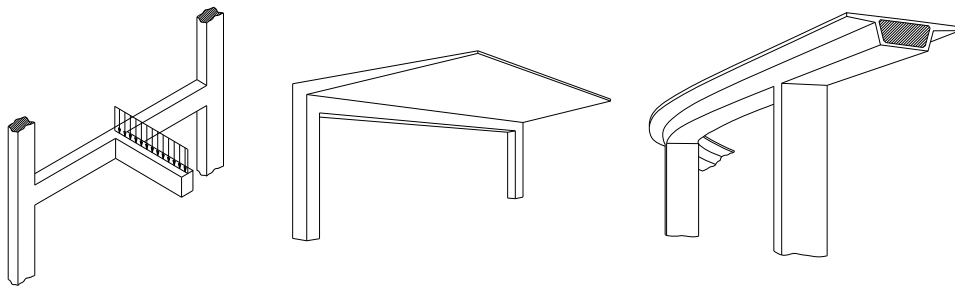


Fig. 1 Examples of current structures with axially restrained beams

From this point of view, the behaviour of axially restrained RC beams under torsion should be similar to PC beams under torsion and the extension of VATM for PC beams could be considered valid for axially restrained beams. However, the longitudinal compressive stress state in axially restrained beams under torsion is different to the same one in PC beams. In these latter, after the decompression of concrete, the initial compressive stress due to prestress disappears and the beam behaves like a common RC beam (prestressing steel behaves like additional ordinary reinforcement steel). In axially restrained beams, the longitudinal compressive stress will only appear after the cracking of the concrete and will increase until the maximum torque is reached. This is because beam's elongation (in the longitudinal direction) only occurs in the cracked stage due to the high tensile stresses in the longitudinal reinforcement in the crack zones (in non-cracked stage, experimental results show that the beam's elongation is negligible since the participation of the longitudinal reinforcement is very scarce). Furthermore, the longitudinal compressive stress state is due to the axial restraint provided by the connections to the other structural elements. For this reason, the behaviour of axially restrained RC beams under torsion cannot be directly extrapolated from the behaviour of PC beams under torsion and VATM should be specifically modified for axially restrained RC beams.

2. Research significance

Very few studies focused on axially restrained RC beams were found in the recent literature. These studies only focus simply supported beams with rectangular section and under flexure. For instance, in the study from Lou *et al.* (2011), the axial restraint was experimentally simulated with external reinforcement located in the tensile zone of the cross section. When compared with RC beams without axial restraint, axially restrained RC beams show higher flexural strength and higher flexural stiffness in cracked stage. This observation shows the favorable influence of the axial restraint on the flexural resistance of RC beams. However, it was also observed that flexural ductility is slightly reduced. No influence of axial restraint on cracking bending moment and on flexural stiffness in non-cracked stage was observed. This is obviously because the beam's elongation (in the tensile zone of the cross section) is only relevant after the cracking of the concrete. The study of Lou *et al.* (2011) also shown that the tensile force in the external reinforcement increases linearly, from the cracking bending moment up to the failure of the beam.

No studies (theoretical or experimental) specially focused on axially restrained RC beams under torsion were found in the consulted literature.

As previously referred in Section 1, it is expected that torsional strength of RC beams also increases due to axial restraint. For torsion design, the current codes of practice don't incorporate specific clauses to compute the favorable effect due to longitudinal compressive stresses. Furthermore, a theoretical and reliable model still does not exist to predict the ultimate behaviour, namely the effective torsional strength, of axially restrained RC beams under torsion. These aspects make this study particularly important, because a simple calculus procedure will allow to optimize the design of RC beams under torsion.

This article presents a computing procedure developed to predict the torsional strength of axially restrained RC beams. This computing procedure is based on a modification of the VATM to account for the influence of the variable longitudinal compressive stress state due to the axial restraint conditions provided by the connections of the beams to other structural elements. As previously referred, it was observed that the axial restraint modifies the post-cracking stage

behavior of RC beams under flexure. Based in this observation and in its physical explanation, similar effects should be expected for RC beams under torsion. Since this study is mainly focused in the ultimate behaviour of beams under torsion, then VATM will be used to be modified to account for the influence of the axial restraint (VATM provides very good results for high loading levels). It is expected that the modification of VATM will allow to compute the effective ultimate behaviour, namely the torsional strength, of axially restrained RC beams under torsion.

It should be noted that this article only deals with RC beams with rectangular sections (plain or hollow). For such kind of sections, torques are essentially resisted through a circulatory flow of tangential stresses due to torsion (circulatory torsion or St. Venant torsion). Some warping can also exist, mainly in zones when the out of plane deformation of the section is restrained (for instance due to the connection to other structural elements or due to the presence of diaphragms in hollow sections). Several parameters control the response of the member to warping, such as the wall's thickness, dimensions and height to width ratio of the cross section, structural model of the member and loading type (Waldren 1988). The incorporation of the effects of warping is not easy to account and some complicated models exist for RC Members (CEB 1995).

For RC members with rectangular sections (plain or hollow) in non-cracked stage, warping, if restrained, can locally increase the stiffness of the members. This can affect the torsional capacity of the member (Waldren 1988). However, in cracked stage, and mainly in the ultimate behavior, the effects of warping can be highly reduced. This is because the cracks somewhat release the initial restriction and allow the out of plane deformation of the section (Waldren 1988). This explains why satisfactory and simplest design methods for the ultimate limit state to consider the effect of warping in current RC members are not yet incorporated into codes of practice.

The referred above is also stated in important codes of practice such as European codes (Eurocode 2, Model Code 1990, Model Code 2010). In fact, these codes state that for current RC sections (plain or hollow), the effect of warping can be neglected for the design for the ultimate limit state.

In this article the principal purpose is to study the ultimate behaviour of axially restrained RC beams under torsion (with rectangular plain and hollow sections). In this stage the beams are fully cracked. For these reason, the influence of warping was not explicitly considered in this study.

Finally, it should be also pointed out that this study deals exclusively with pure torsion. In actual structures, the interaction between torsion and other internal forces is a common situation. However, the behaviour of members under pure torsion needs to be well known and theoretical and reliable models for pure torsion are still need. Such models can be very useful to be applied in other studies focused in more complex situations with members under interaction forces (for instance, Belarbi *et al.* 2009, Valipour and Foster 2010).

3. Modification of the VATM for RC axially restrained beams

This section describes the steps that lead to the modified formulation of the VATM for axially restrained RC beams under torsion. The general steps that lead to the modified equilibrium formulation of the VATM follow in a very similar way some of the steps used by Hsu and Mo (1985a, 1985b). In these studies the authors derived the VATM for RC beams and when they modified the VATM for PC beams (longitudinal uniform prestress) under torsion, and also some of the steps used by Hsu 1984 when he modified the VATM in order to include “torsion + longitudinal axial force” interaction. In such studies, the axial force was considered as an “external

force” to be equilibrated by the longitudinal reinforcement. In the present study the influence of the axial force due to axial restraint for equilibrium is considered in the same way as the one presented by the referred articles, in order to modify the formulation of VATM for axially restrained RC beams under torsion. It should be also stated that the general steps that lead to modify the compatibility formulation of the VATM follow in a similar way some of the steps used by Hsu and Mo (1985b). In this study the authors derived the VATM for PC beams (longitudinal uniform prestress) under torsion and also some of the steps used by Bernardo *et al.* (2012b) to extend the VATM for low level loading stages, in order to consider the initial deformation state due to initial and longitudinal compressive stresses. In this article, only the parts specifically related with the behaviour of axially restrained RC beams are presented in detail. More details about the unchanged parts of the VATM, valid for axially restrained RC beams, are not presented here in order to not be repeated and to not overload the article, these can be found in the referenced articles.

As it will be presented and explained in Section 4, only some experimental results with PC beams under torsion were found in the consulted literature, which are able to be used as beams with axial restraint for comparison purpose. For this reason, in this article the modified VATM include the extension for PC beams under torsion (only longitudinal uniform prestress will be considered). It should be noted that VATM for RC beams constitutes a particular case of VATM for PC beams, when neither prestress force nor prestress reinforcement exists.

3.1 Methodology to incorporate the influence of axial restraint

Fig. 2(a) shows a general case of a RC beam under torsion incorporated into a simple frame and rigidly connected to columns. After the cracking of the concrete, the beam’s length tends to increase. The elongation of the beam mobilizes the flexural stiffness of the columns, which in turn will restrain the free elongation of the beam. The level of axial restraint will depends on the level of beam’s elongation and also on the level of flexural stiffness of the columns.

In this study, it is assumed that the total free elongation of the beam (without axial restraint), Δl , can be computed from the tensile strain in the longitudinal reinforcement, ε_l . In other words, it is assumed that the total free elongation of the beam is equal to the total elongation of the longitudinal reinforcement. This hypothesis can be state from earlier experimental observations (Hsu 1968). In this study, it is also assumed that the tensile strain in the longitudinal reinforcement, computed from the VATM, can be considered constant in all the beam’s length (l). This hypothesis is acceptable since the torsional cracks pattern in fully cracked RC beams, as observed in experimentally studies (Bernardo and Lopes 2009), shows multiple helical cracks in all the beam’s length. Then, it can be state that all the sections of the beam are in cracked stage. It should be noted that this hypothesis is consistent with VATM assumption, which assumes that the beam is fully cracked. Then, the tensile strain in the longitudinal reinforcement can be computed directly from the VATM.

Based on the above, the total elongation of the beam (without axial restraint) can be computed from (Fig. 2(b))

$$\Delta l = l\varepsilon_l \quad (1)$$

In the beam’s model illustrated in Fig. 2(b) (isolated beam), the influence of the axial restraint provided by the flexural stiffness of the columns can be simply simulated with linear springs

located in the top sections of the beam (Fig. 2(c)). Due to the springs' stiffnesses (assumed here to be different and equal to k_1 and k_2), an axial and centered force (F_c) will be applied in the beam as the result of the beam's elongation. This force will be proportional to the free beam's elongation (Δl) and to the stiffnesses of the connection in the top sections (k_1 and k_2), and will reduce the free beam's elongation (Fig. 2(c)). Then, in order to study the torsional behaviour of axially restrained RC beams, an interaction force situation ($F_c + T$) must be considered. From Fig. 2(c), being $k_1 \neq k_2$, then $\Delta l_1 \neq \Delta l_2$ (being $\Delta l = \Delta l_1 + \Delta l_2$). From longitudinal equilibrium, the restoring forces from the springs $F_{c1} = k_1 \Delta l_1$ and $F_{c2} = k_2 \Delta l_2$ must be equal. This force is called F_c and is computed as follows

$$F_c = k_1 \Delta l_1 = k_2 \Delta l_2 \quad (2)$$

In this study, the stiffnesses at the top sections of beams will be considered as an initial input data for the calculus procedure presented in sections below. These parameters should be previously defined by the user and should be computed as a function of the real characteristics of the beam's connection to the other structural elements. A constant value can be assumed for the stiffnesses, or even a non-constant value (function of Δl) if a nonlinear analysis is assumed (for instance to account for the cracking of the concrete in the other structural elements).

3.2 Beam element under shear, bending and compressive axial force

As previously referred, to study the torsional behaviour of axially restrained RC beams, an interaction force situation ($F_c + T$) must be considered. Fig. 3 shows a simply supported beam with a thin section (t), under a concentrated force at mid span and also an axial compressive force F_c due to the axial restraint. Fig. 3 also shows an internal beam element under a constant shear force V , a variable bending moment M and the axial compressive force F_c (general equilibrium situation). In this section, the force F_c will be considered as an external force to be equilibrated by the internal forces V , D and \bar{N} .

VATM assumes that all the longitudinal steel is concentrated in the top and bottom stringers (Hsu 1984 and Hsu and Mo 1985a). The distance between the stringers is d_v . The longitudinal length of the beam element, $d_v \cot \alpha$, corresponds to the horizontal projection of a crack inclined at an angle α . In the right face, the shear flow $q = V / d_v$ induced by the shear force V is illustrated. The internal forces (V , D and \bar{N}) in the concrete are illustrated in the left face of the beam element. The compressive force D in the diagonal concrete strut is applied on an inclined transversal section with width t and height $d_v \cos \alpha$ (Fig. 3).

From the force triangle illustrated in Fig. 3, the shear force V can be divided into two components: the total force in the longitudinal reinforcement \bar{N} and the compressive force D . The force \bar{N} should be taken equally by the top and bottom longitudinal steel and must also account for the external compressive axial force F_c

$$\bar{N} = V \cot \alpha - F_c \quad (3)$$

The compressive force D and the corresponding stress σ_d in the diagonal concrete strut are given as follows (from the original VATM, Hsu 1984)

$$D = \frac{V}{\sin \alpha} \quad (4)$$

$$\sigma_d = \frac{D}{t d_v \cos \alpha} \quad (5)$$

All the remaining equations from VATM for a beam element under a constant shear force V and a variable bending moment M (Hsu 1984) remain unchanged for beams with axial compressive force F_c due to the axial restraint. These equations are not presented here because they are not necessary for the next sections.

3.3 Hollow beam element under torsion

Fig. 4 shows a rectangular hollow beam element (with symmetrical ordinary longitudinal reinforcement in the corners and with symmetrical prestress longitudinal reinforcement in the walls) under a torsional moment T and an additional external axial compressive force F_c due to the axial restraint. VATM states that, in each internal section, two forces are observed: the forces in the longitudinal bars and the forces in the diagonal concrete struts with an angle α to the horizontal (Hsu 1984). The resultant of these two forces is the shear flow q in the transversal section plane, which coincides with the center line of the effective wall thickness, t_d , and which can be related with the torsional moment T and the area A_o limited by the center line of the flow of shear stresses (which coincides with the center line of the wall thickness, t_d) from Bred's Thin Tube Theory (Hsu 1984)

$$q = \frac{T}{2A_o} \quad (6)$$

In each wall of the hollow beam, the shear force V is defined as the resultant force of the shear flow q along the length of each wall l_q (defined as the length of the center line of the flow of shear stresses, see Fig. 4)

$$V = q l_q \quad (7)$$

The shear force V from Eq. (7) is similar to the shear force acting on the thin section of the beam element of Fig. 3, so it is assumed that each wall of the hollow section behaves like the referred thin section under the shear force V . Then, from Eq. (3), it can be state that, for each wall of the hollow beam of Fig. 4 and assuming that the external compressive axial force F_c is equally distributed by the longitudinal reinforcement in each wall, the total force in the longitudinal reinforcement is

$$\bar{N} = q l_q \cotg \alpha - \frac{F_c}{4} \quad (8)$$

In Eq. (8), the external force F_c is divided by the 4 walls of the hollow beam.

From Fig. 4, it can be also state that the longitudinal compressive force F_c only modifies the equilibrium equations in the longitudinal direction and must be supported by the longitudinal reinforcement. Defining $\Delta N = \sum \bar{N}$ as the total longitudinal force in the longitudinal

reinforcement in the overall section and $p_o = \sum l_q$ as the perimeter of the center line of the flow of shear stresses, from Eq. (8) it can be state that

$$\Delta N = qp_o \cotg \alpha - F_c \quad (9)$$

After the decompression of concrete, a PC beam under torsion behaves like a common RC beam. Thus, prestress only influence equilibrium equations in the prestress direction (longitudinal). Then, total longitudinal force in the reinforcement should include both ordinary and prestress reinforcement (Hsu and Mo 1985b). For PC beams with longitudinal prestress, the total longitudinal force in the reinforcement is

$$\Delta N = A_l \sigma_l + A_{pl} \sigma_{pl} \quad (10)$$

Where:

A_l ; A_{pl} = total area of the ordinary and prestress longitudinal reinforcement, respectively;

σ_l ; σ_{pl} = stress in the ordinary and prestress longitudinal reinforcement, respectively.

Equating Eq. (9) to Eq. (10) and substituting q from Eq. (6) leads to:

$$A_l \sigma_l + A_{pl} \sigma_{pl} = \frac{T p_o}{2A_o} \cotg \alpha - F_c \quad (11)$$

Computing the theoretical $T - \theta$ curve from the original VATM for PC beams under torsion (without F_c) requires the three following equilibrium equations to compute the torque, T , the effective thickness of the concrete struts, t_d , of the equivalent tubular section and the angle of the concrete struts, α , from the longitudinal axis of the beam (Hsu and Mo 1985b)

$$T = 2A_o t_d \sigma_d \sin \alpha \cos \alpha \quad (12)$$

$$\cos^2 \alpha = \frac{A_l \sigma_l + A_{pl} \sigma_{pl}}{p_o \sigma_d t_d} \quad (13)$$

$$t_d = \frac{A_l \sigma_l + A_{pl} \sigma_{pl}}{p_o \sigma_d} + \frac{A_t \sigma_t}{s \sigma_d} \quad (14)$$

Where

A_t = area of one leg of the transversal reinforcement;

σ_t = stress in the transversal reinforcement;

s = longitudinal spacing of the transversal reinforcement.

Eq. (12) comes from Eqs. (4) and (5) and also from Eq. (6). Then, Eq. (12) remains valid for beams with axial restraint. Eqs. (13) and (14) are written as function of the longitudinal force in the reinforcement ($A_l \sigma_l + A_{pl} \sigma_{pl}$), then they must be corrected in order to incorporate the external compressive axial force F_c . Substituting Eq. (12) into Eq. (11), gives Eq. (15) that must replace Eq. (13) in order to be used for beams with axial restraint.

$$\cos^2 \alpha = \frac{A_l \sigma_l + A_{pl} \sigma_{pl} + F_c}{p_o \sigma_d t_d} \quad (15)$$

Following the same previous reasoning, Eq. (12) must be replaced by Eq. (16) in order to be used for beams with axial restraint.

$$t_d = \frac{A_l \sigma_l + A_{pl} \sigma_{pl} + F_c}{p_o \sigma_d} + \frac{A_t \sigma_t}{s \sigma_d} \quad (16)$$

Computing the theoretical $T - \theta$ curve from the original VATM for PC beams under torsion (without F_c) also requires the three following compatibility equations to compute the strain of the longitudinal reinforcement, ε_l , the strain of the transversal reinforcement, ε_t , and the twist, θ (Hsu and Mo 1985b)

$$\varepsilon_l = \left(\frac{A_o^2 \sigma_d}{p_o T \cotg \alpha} - \frac{1}{2} \right) \varepsilon_{ds} \quad (17)$$

$$\varepsilon_t = \left(\frac{A_o^2 \sigma_d}{p_o T \tg \alpha} - \frac{1}{2} \right) \varepsilon_{ds} \quad (18)$$

$$\theta = \frac{\varepsilon_{ds}}{2t_d \sin \alpha \cos \alpha} \quad (19)$$

Since Eq. (17) to Eq. (19) are not written as function of the longitudinal force in the reinforcement ($A_l \sigma_l + A_{pl} \sigma_{pl}$), then they should remain valid for beams with axial restraint. However, for axially restrained RC beams the compressive strain in the outer fiber of the concrete strut ε_{ds} (Fig. 4) must be replaced by the effective compressive strain $\varepsilon_{ds,ef}$ to account for the axial restraint. Parameter $\varepsilon_{ds,ef}$ will be estimated as follows.

As illustrated in Fig. 2, the longitudinal force F_c will reduce the free beam's elongation, then the effective strain in the concrete strut in axially restrained RC beams is lesser than the same one in free beams. From Eq. (2) the axial force F_c can simply be estimated from the elongation ΔL (being $\Delta L = \Delta l_1 + \Delta l_2$) of the free beam (without axial restraint). If the beam is prestressed, the initial force in concrete due to the longitudinal prestress (F_{ci} , see Eq. (21)) induces an initial shortening in the beam. Then, F_{ci} must also be considered in addition to F_c .

Under F_c (or $F_c + F_{ci}$ for PC beams), the free beam will suffer a longitudinal shortening. This shortening can be computed by following the same reasoning and assumptions from Hsu and Mo, 1985b when they derived the VATM for PC beams (longitudinal uniform prestress) under torsion and also the same ones used by Bernardo *et al.* (2012b) to extend the VATM for low level loading stages, in order to consider the initial deformation state due to initial and longitudinal compressive stresses.

As previously referred in Section 3.2, it is assumed that the beam's shortening (due to F_c) is equal to the shortening of the longitudinal reinforcement $\varepsilon_{l,c}$. This latter can simply be estimated from

$$\varepsilon_{l,c} = \frac{\sigma_c}{E_c} = \frac{F_c + F_{ci}}{E_c A_{ch}} = \dots = \frac{F_c + F_{ci}}{E_c (A_c - A_h - A_{pl}) + A_{sl} (E_s - E_c)} \quad (20)$$

$$F_{ci} = \sigma_{pi} A_{pl} \quad (21)$$

Where:

- A_{ch} = equivalent area of concrete (homogenized concrete section);
- $E_c; E_s$ = Young's Modulus for concrete and ordinary reinforcement, respectively;
- σ_c = concrete compressive stress due to F_c ;
- A_c = area limited by the outer perimeter of the section;
- A_h = hollow area (for plain sections: $A_h = 0$).

The shortening of the beam also induces a shortening in the outer fiber of the diagonal concrete strut, $\varepsilon_{ds,c}$. This latter can be calculated from $\varepsilon_{l,c}$ (Eq. (22) and Fig. 5).

$$\varepsilon_{ds,c} = \frac{\varepsilon_{l,c}}{\cos \alpha} \quad (22)$$

For each level of the longitudinal axial force F_c , the effective compressive strain $\varepsilon_{ds,ef}$ is computed as follows

$$\varepsilon_{ds,ef} = \varepsilon_{ds} + \varepsilon_{ds,c} \quad (23)$$

In Eqs. (17) to (19), the compressive strain in the outer fiber of the concrete strut, ε_{ds} , must be replaced by the effective compressive strain, $\varepsilon_{ds,ef}$, in order to account for the axial restraint.

As referred latter (Section 3.5), the methodology previously presented to correct the compressive strain in the concrete strut to account for the axial restraint allow to maintain the original structure of the iterative calculation procedure of VATM.

The strain at the surface of the diagonal concrete strut, ε_{ds} (Fig. 4), and at the centre line of the flow of shear stresses, $\varepsilon_d = \varepsilon_{ds} / 2$ (Fig. 4), can be computed from (Hsu and Mo 1985a)

$$\varepsilon_{ds} = \frac{2p_o t_d}{A_o} (\varepsilon_t + \varepsilon_d) \operatorname{tg} \alpha \sin \alpha \cos \alpha \quad (24)$$

The procedure to compute the strain in the longitudinal prestress reinforcement, ε_{pl} , to compute subsequently the stress σ_{pl} , is the following one (Hsu and Mo 1985b)

$$\varepsilon_{pl} = \varepsilon_{dec,l} + \varepsilon_l \quad (25)$$

$$\varepsilon_{dec,l} = \varepsilon_{pi,l} + \varepsilon_{li} \quad (26)$$

$$\varepsilon_{pi,l} = \sigma_{pi,l} / E_p \quad (27)$$

$$\varepsilon_{li} = \frac{A_{pl} \sigma_{pi,l}}{A_l (E_s - E_c) + (A_c - A_h - A_{pl}) E_c} \quad (28)$$

Where

- $\varepsilon_{dec,l}$ = strain in the longitudinal prestress reinforcement at decompression;
- ε_{li} = inicial strain in the longitudinal ordinary reinforcement;
- $\varepsilon_{pi,l}$ = inicial strain in the longitudinal prestress reinforcement;
- $\sigma_{pi,l}$ = initial stress in the longitudinal prestress reinforcement;
- E_p = Young's modulus of the longitudinal prestress reinforcement.

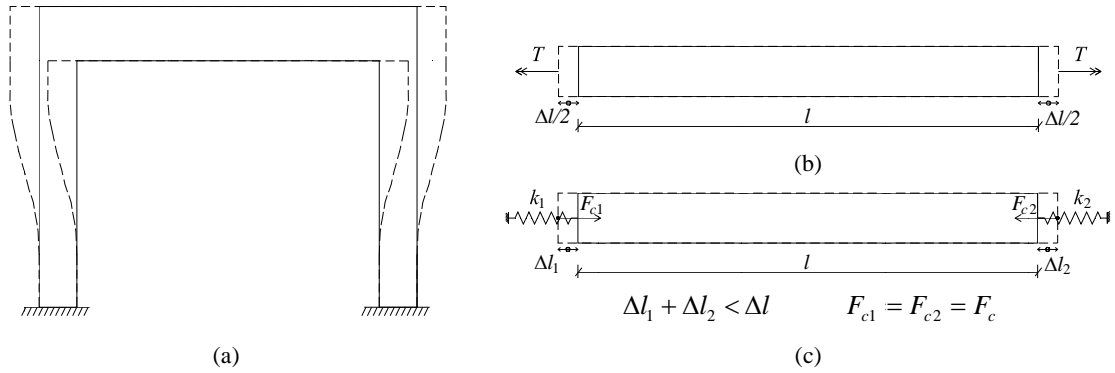


Fig. 2 Axially restrained RC beam: (a) real condition - (b) free condition - (c) idealized condition

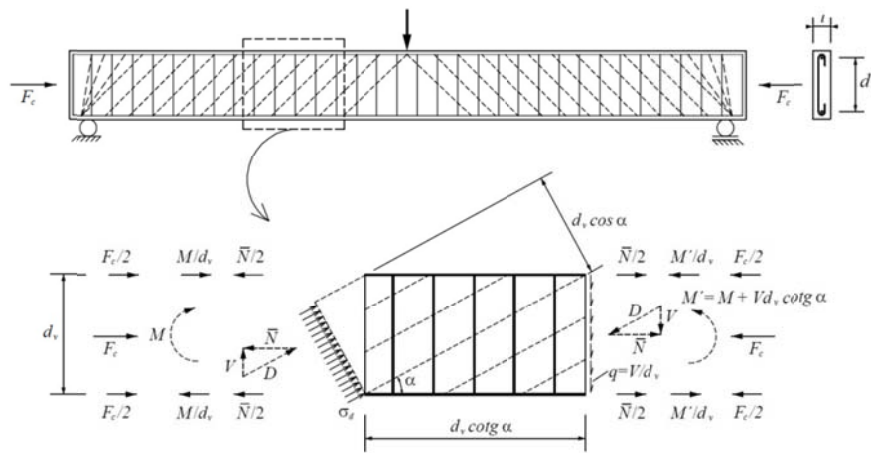


Fig. 3 Equilibrium of a beam under shear, bending and axial compressive force

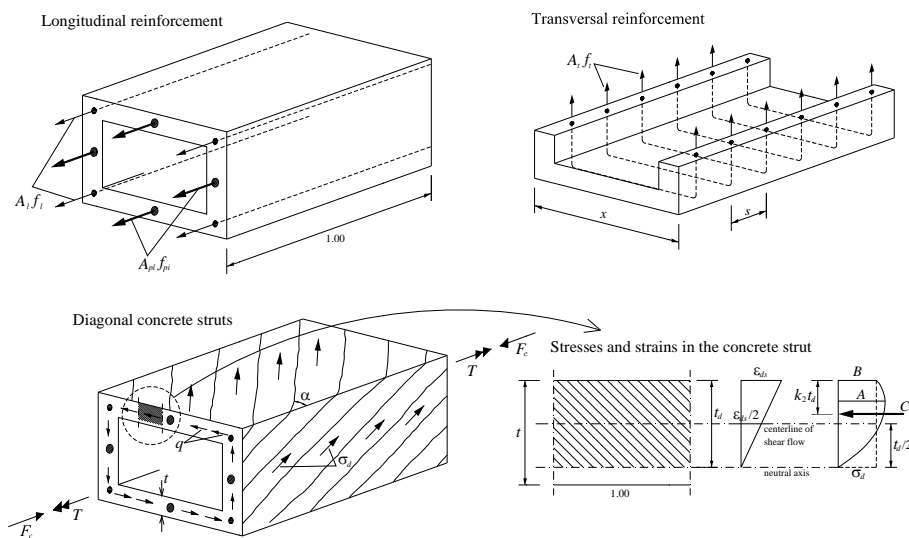


Fig. 4 Equilibrium of a rectangular hollow beam element under torsion

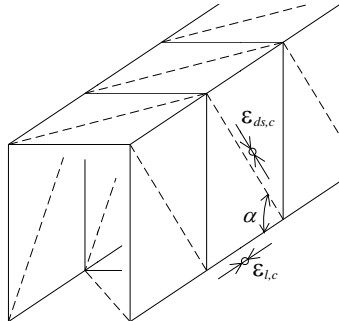


Fig. 5 Shortening of the diagonal concrete strut due to axial restraint (truss model)

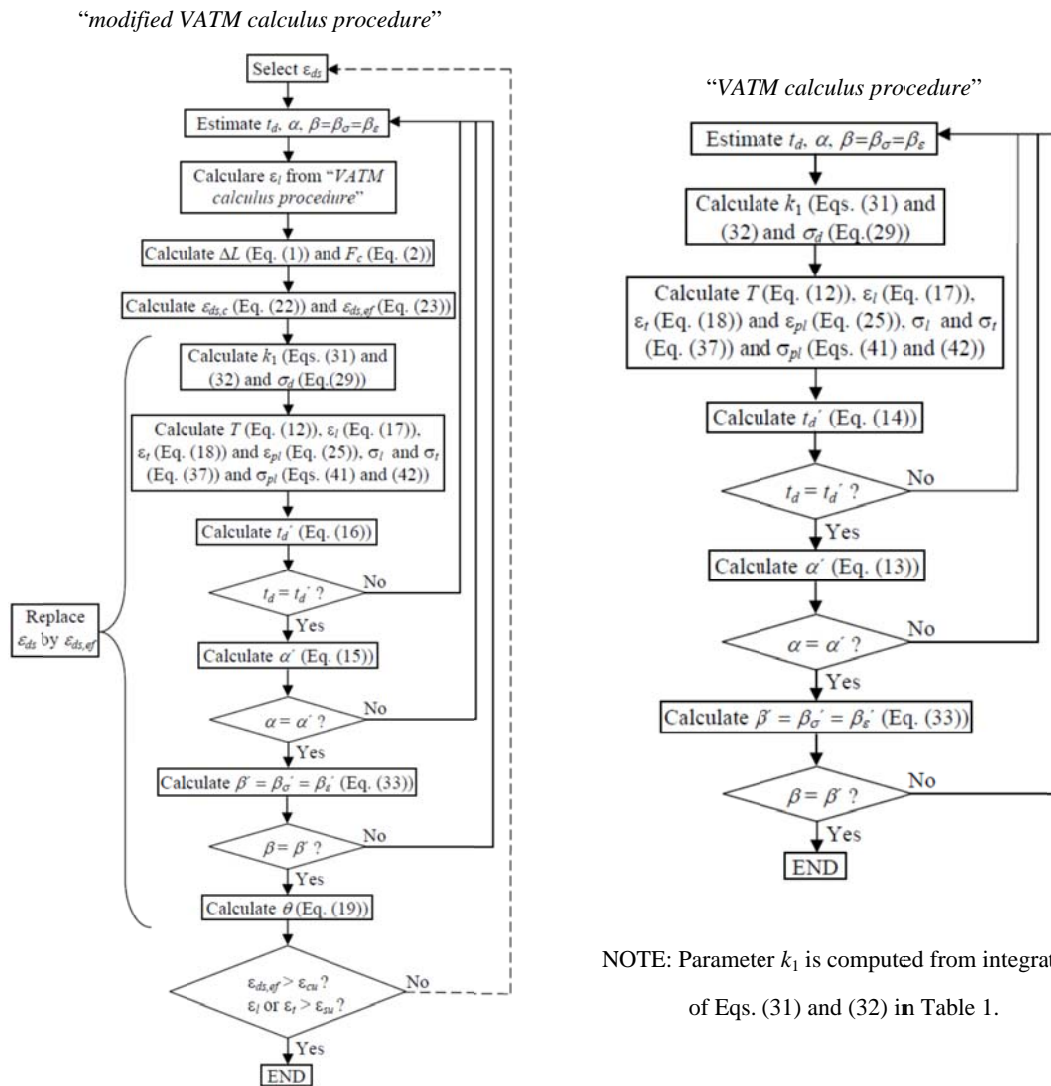


Fig. 6 Flowcharts for the calculation of $T - \theta$ curves

Table 1 Nonlinear σ - ε relationships for materials

Concrete in compression in the struts:

 (Belarbi and Hsu 1991, Hsu and Zhang 1997, Zhang and Hsu 1998, Bernardo *et al.* 2012a)

$$\sigma_d = \beta_\sigma f'_c \left[2 \left(\frac{\varepsilon_d}{\beta_\varepsilon \varepsilon_o} \right) - \left(\frac{\varepsilon_d}{\beta_\varepsilon \varepsilon_o} \right)^2 \right] \quad \text{if } \varepsilon_d \leq \beta_\varepsilon \varepsilon_o \quad (31)$$

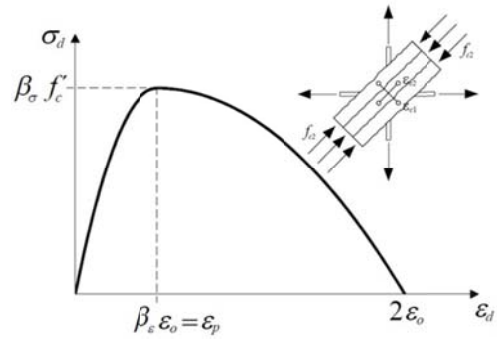
$$\sigma_d = \beta_\sigma f'_c \left[1 - \left(\frac{\varepsilon_d - \beta_\varepsilon \varepsilon_o}{2\varepsilon_o - \beta_\varepsilon \varepsilon_o} \right)^2 \right] \quad \text{if } \varepsilon_d > \beta_\varepsilon \varepsilon_o \quad (32)$$

$$\beta_\sigma = \beta_\varepsilon = \frac{R(f'_c)}{\sqrt{1 + \frac{400\varepsilon_{c1}}{\eta'}}} \quad (33)$$

$$\eta = \frac{\rho_l f_{sy,l}}{\rho_t f_{sy,t}} \quad (34)$$

$$\begin{cases} \eta \leq 1 \Rightarrow \eta' = \eta \\ \eta > 1 \Rightarrow \eta' = 1/\eta \end{cases} \quad (35)$$

$$R(f'_c) = \frac{5.8}{\sqrt{f'_c (\text{MPa})}} \leq 0.9 \quad (36)$$


Ordinary reinforcement in tension ($\sigma \equiv f$):

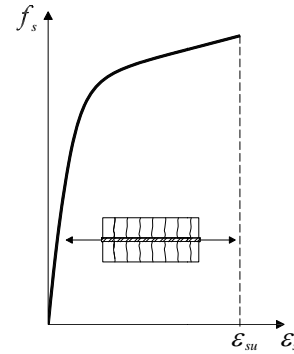
(Belarbi and Hsu 1994)

$$f_s = \frac{0.975 E_s \varepsilon_s}{\left[1 + \left(\frac{1.1 E_s \varepsilon_s}{f_{sy}} \right)^m \right]^{\frac{1}{m}}} + 0.025 E_s \varepsilon_s \quad (37)$$

$$m = \frac{1}{9B - 0.2} \leq 25 \quad (38)$$

$$B = \frac{1}{\rho} \left(\frac{f_{cr}}{f_{sy}} \right)^{1.5} \quad (39)$$

$$f_{cr} = 0.3114 \sqrt{f'_c} (\text{MPa}) \quad (40)$$

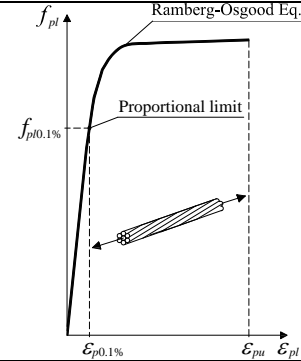


Prestress reinforcement in tension ($\sigma \equiv f$):

(Ramberg-Osgood 1943, Hsu and Mo 1985b)

$$f_p = E_p \varepsilon_p \quad \text{if} \quad \varepsilon_p \leq \varepsilon_{p0.1\%} = f_{p0.1\%} / E_p \quad (41)$$

$$f_p = \frac{E_p \varepsilon_p}{\left[1 + \left(\frac{E_p \varepsilon_p}{f_{pt}} \right)^{4.38} \right]^{\frac{1}{4.38}}} \quad \text{if} \quad \varepsilon_p > \varepsilon_{p0.1\%} \quad (42)$$



The stress of the concrete struts, σ_d , is defined as the medium stress of a non-uniform diagram (Fig. 4)

$$\sigma_d = k_1 \beta_\sigma f'_c \quad (29)$$

Where:

β_σ = reduction coefficient for the stress to account for the softening effect;

k_1 = ratio between the medium stress (B , see Fig. 4) and the maximum stress (A , see Fig. 4);

f'_c = average concrete compressive strength.

The k_1 parameter is an average stress and it can be obtained by integrating the $\sigma - \varepsilon$ relationship of the compressive concrete in the struts (Eqs. (31) and (32) in Table 1). In this study, parameter k_1 will be calculated by numerical integration.

3.4 Nonlinear stress (σ) – strain (ε) relationships for the materials

Usually, theoretical models for the behaviour of cracked RC elements under shear consider the independent behaviour of the concrete and of the reinforcement through their average $\sigma - \varepsilon$ relationships. For concrete in compression in the struts, the average nonlinear $\sigma - \varepsilon$ relationships usually account for the softening effect (influence of the transversal tension strains) by incorporating reduction factors. For reinforcement in tension, some average (smeared) nonlinear $\sigma - \varepsilon$ relationships account for the stiffening effect (interaction between reinforcement and concrete in tension between cracks). Other simplified $\sigma - \varepsilon$ relationships (bilinear) do not incorporate this interaction and are defined from uniaxial tensile tests.

In the last two decades, several $\sigma - \varepsilon$ relationships for concrete in compression and for ordinary reinforcement in tension were proposed by authors. For this reason, Bernardo *et al.* (2012a) tested several $\sigma - \varepsilon$ relationships for the materials in order to compute the ultimate behaviour of RC beams under torsion by using VATM formulation. Among the tested models and based on several comparative analyses with experimental results, the authors found one theoretical model that provides very good predictions for the torsional strength. This theoretical model incorporates the $\sigma - \varepsilon$ relationship for compressed concrete in struts proposed by Belarbi and Hsu (1991) with softening factors proposed by Hsu and Zhang (1997) and Zhang and Hsu (1998). These $\sigma - \varepsilon$ relationship will also be used in this study. It should be noted that this $\sigma - \varepsilon$ relationship for concrete in compression was meant for fixed-angle truss-model theories. However, several authors further incorporated in their models, based on variable angle truss-models, the same, or similar

versions, of the $\sigma - \varepsilon$ relationship for concrete in compression employed in this study (for instance, Hsu and Zhang 1997, Zhang and Hsu 1998, Hsu and Zhu 2002, Jeng and Hsu 2009, Bernardo *et al.* 2012b, Bernardo *et al.* 2014). In these studies the authors found that such $\sigma - \varepsilon$ relationship was shown to be adequate also for models based on variable angle truss-models.

Table 1 presents the mathematical equations for the $\sigma - \varepsilon$ relationship for concrete in compression in struts (Eqs. (31) and (32)) as well as the mathematical equations for the reduction factors for stress (β_σ) and strain (β_ε) (Eqs. (33)-(36)). The meanings of the principal parameters in Table 1 for the $\sigma - \varepsilon$ relationship for concrete are: ε_o is the strain corresponding to the peak stress (f'_c), ε_{c1} is the principal tension strain ($\varepsilon_{c1} = \varepsilon_l + \varepsilon_t + \varepsilon_d$, Hsu 1984), $\varepsilon_c = \varepsilon_{c2}$ is the compression strain in the principal direction of the compression stress ($f_c = f_{c2}$) and η represents the ratio between the resisting forces in the longitudinal and transversal reinforcement.

For PC beams, parameter η should also account for the resistance force in the longitudinal prestressed reinforcement (Eq. (30)).

$$\eta = \frac{\rho_l f_{sty} + \rho_{pl} f_{pl0.1\%}}{\rho_t f_{sty}} = \frac{A_l f_{sty} + A_{pl} f_{pl0.1\%}}{u A_t f_{sty} / s} \quad (30)$$

Where:

ρ_l ; ρ_t = longitudinal and transversal ordinary reinforcement ratio ($\rho_l = A_{sl} / A_c$ and $\rho_t = A_{st} u / (A_c s)$ with $A_c = xy$, being x and y the external dimensions of the rectangular section);

ρ_{pl} = longitudinal prestress reinforcement ratio ($\rho_{pl} = A_{pl} / A_c$);

u = perimeter of the transversal ordinary reinforcement ($u = 2x_1 + 2y_1$ with x_1 and y_1 the minor and major dimension of the hoop);

f_{sly} ; f_{sty} = yielding stress of the longitudinal and transversal ordinary reinforcement, respectively;

$f_{pl0.1\%}$ = conventional stress of the longitudinal prestress reinforcement.

In their comparative analyzes Bernardo *et al.* (2012a) also tested several $\sigma - \varepsilon$ relationships for the reinforcement in tension. Among the tested models the authors found that the best $\sigma - \varepsilon$ relationship for the reinforcement in tension to compute the ultimate behaviour of RC beams under torsion by using VATM formulation, is the average $\sigma - \varepsilon$ relationship for ordinary rebars under tension proposed by Belarbi and Hsu (1994). This relationship accounts for the tensile stress that is absorbed by concrete in tension between cracks (stiffening effect). For this reason, the theoretical model used in this study also incorporates this average $\sigma - \varepsilon$ relationship for the tensile steel bars embedded in concrete (ordinary reinforcement).

To characterize the prestressing steel in tension, a tensile $\sigma - \varepsilon$ relationship for bare prestressing strands can be used since the decreased stress in embedded tendons compared with bare strands is less significant than in embedded mild steel compared with bare steel bars (Wang 2006). Then, a $\sigma - \varepsilon$ relationship based on the equation of Ramberg-Osgood (1943) can be used. Hsu and Mo 1985b showed that this relationship is adequate for current prestressing steel. The strain in the longitudinal prestressing steel should be computed considering the initial stress due to prestressing (Eqs. (25) to (28)). The previously referred $\sigma - \varepsilon$ relationship for prestress steel in tension is also used in this study.

Table 1 presents the mathematical equations for the $\sigma - \varepsilon$ relationship for ordinary reinforcement in tension (Eqs. (37) to (40)) and for the $\sigma - \varepsilon$ relationship for prestress

reinforcement (Eqs. (41) and (42)). The meanings of the principal parameters in Table 1 for the $\sigma - \varepsilon$ relationships for reinforcement are: f_s and f_p are the tensile stress, f_{sy} is the yielding stress, $f_{p0.1\%}$ is the stress correspondent to the conventional strain $\varepsilon_{p0.1\%} = 0.1\%$, f_{st} and f_{pt} are the tensile strength, f_{cr} is the tensile strength of the concrete, ρ is the reinforcement ratio, ε_s and ε_p are the tension strain, ε_{sy} is the yielding strain at the end of the elastic behaviour, ε_{su} and ε_{pu} are the ultimate strain.

3.5 Computation of the Torque (T) - Twist (θ) Curve

The computation of the $T - \theta$ curves based on VATM requires an iterative computation procedure since the variables t_d , α and $\beta_\sigma = \beta_\varepsilon$ are initially unknown and interdependent. In the original VATM the input variable is ε_{ds} (Hsu and Mo 1985a, Bernardo *et al.* 2012). In order to maintain the structure of the original and efficient iterative calculus procedure from VATM, ε_{ds} should remain the input variable. The iterative procedure for the modified VATM in order to include axially restrained RC beams and PC beams under torsion is presented in Fig. 6. In a first step, for each ε_{ds} input value, the original VATM calculus procedure is used to compute the response of the RC or PC beam under torsion without axial restraint (free beam's condition), namely to compute the strain in the longitudinal reinforcement, ε_l . Based on this value, the beam's elongation ΔL and the longitudinal force F_c (due to the axial restraint) are computed. Then, the effective compressive strain in the outer fiber of concrete strut $\varepsilon_{ds,ef}$ is computed and the calculus procedure for the modified VATM is started.

Based on the global calculus procedure presented in Fig. 6, a computing tool based on VATM and previously developed with the help of the computing programming language Delphi to compute the $T - \theta$ curve for RC and PC beams under torsion (Andrade *et al.* 2011) was modified in order to include axially restrained RC beams under torsion. For RC beams, parameters A_{pl} and $f_{pi,l}$ must be considered null. In order to account for the distinction between the behavior between PC beams and axially restrained RC beams under torsion, as explained in Section 1 and Sections 3.1 to 3.4 the computing tool previously developed by the authors for RC and PC beams under torsion, and extended in this study to include axially restrained RC beams, includes an option for the user in order to choose what type of beams is to be calculated: RC beam, PC beam, axially restrained RC beams or axially restrained PC beams.

The theoretical results obtained with this computing tool will be compared with some experimental results of test beams under pure torsion which are available in the literature and able to be used as axially restrained RC beams (Section 4) and also with some numerical results from nonlinear finite element analysis (Section 5). The comparative analysis will focus on the ultimate behaviour of the beams, namely on the torsional strength.

The theoretical failure of the sections was defined from the conventional maximum strains of the materials (concrete and steel). Either the strain of the concrete struts, ε_{ds} (Fig. 4), reaches its maximum value (ε_{cu}) or the steel strain, ε_s , reaches the usual maximum value of $\varepsilon_s = 10^0/00$. In this study, ε_o and ε_{cu} are calculated from EC2 2010.

4. Comparative analysis with experimental results

In this section, a comparative analysis mainly focused on the ultimate behaviour will be carried

out with the help of some experimental results. In the consulted literature, experimental studies focused on axially restrained RC beams under torsion were not found. However, in PC beams (with uniform longitudinal prestress) if external longitudinal prestress reinforcement is used, then, in addition to the initial compressive stress due to the prestress force, a compressive stress state arises due to the axial restraint provided by the axial stiffness of the prestress reinforcement. Such beams can be studied as axially restrained PC beams under torsion. In this case, the stiffness k to calculate the compressive force is defined as follow

$$k = \frac{E_p A_{pl}}{l_p} \quad (43)$$

Where l_p is the length of the external longitudinal prestress reinforcement between anchorage heads.

In the consulted literature, only two beams were found with the conditions explained previously. Such beams, D1 and D2 from Bernardo 2003 (with 5.9 meters long), have a rectangular hollow cross section and were subjected to pure torsion until failure. The geometry and detailing of the beams are presented in Fig. 7. External prestressing was applied through three (Beam D1) and four (Beams D2) 0.6 inches wires centered in the section (Fig. 7). The ordinary reinforcement used in Beams D1 and D2 were ribbed bars (diameters of 10 and 16 mm) sold commercially as A500 Class. For the elastic modulus of the steel, E_s , the typical value given by different codes was used: 200 GPa. The prestress reinforcement used in Beams D1 and D2 were wires belonging to Class S1670/1860. The modulus of elasticity, E_p , was assumed to be the one indicated by the producer: 195 GPa.

From Fig. 7 it can be state that the axial and centered force of the beams due to the axial restraint provided by the external prestressing reinforcement along all the beam's length is $F_c = k\Delta L$, with k computed from Eq. (43). Eq. (2) cannot be directly used to compute $F_c = k\Delta L$ because the model of the beam is different from the one illustrated in Fig. 2.

Table 2 summarizes the geometrical and mechanical properties of the PC beams D1 and D2, namely: the external width (x) and height (y) of the rectangular cross hollow sections, the thickness of the walls (t), the distances between centerlines of legs of the closed stirrups (x_1 and y_1), the total area of longitudinal reinforcement (A_{sl}), the distributed area of one leg of the transversal reinforcement (A_{st} / s , where s is the spacing of transversal reinforcement), the total area of longitudinal prestress reinforcement (A_{pl}), the longitudinal and transversal ordinary reinforcement ratio (ρ_l and ρ_t), the average concrete compressive strength (f'_c), the average yielding stress of longitudinal and transversal reinforcement (f_{ly} and f_{ty}), the proportional conventional limit stress to 0.1% ($f_{p0,1\%}$), the initial stress in the prestressing reinforcement (f_{pi}) and the average stress in the concrete due to prestressing (f_{cp}). Young's Modulus of concrete (E_c), concrete strain correspondent to peak stress (ε_o) and ultimate compressive concrete strain (ε_{cu}) were calculated from EC2 2010. Ultimate tensile reinforcement value (ε_{su}) was considered equal to 1% (usual conventional value). The axial stiffness k provided by the external longitudinal prestress reinforcement is computed from Eq. (43), with $l_p = 7.12$ m being the distance between anchorage heads (Fig. 7).

By using the computing tool based on the calculus procedure presented in Fig. 6, and based on the properties of the experimental beams D1 and D2 presented in Table 2, the theoretical $T - \theta$ curves for the test beams were calculated. Such curves are presented in Figs. 8(a) and 8(b). Each figure includes two theoretical $T - \theta$ curves and one experimental $T - \theta$ curve. This latter was

drawn from the experimental results of the beams (Bernardo 2003). The first theoretical $T - \theta$ curve was calculated from VATM for PC beams under torsion (“VATM”). Thus, the effect of axial restraint was not considered. The second $T - \theta$ curve was calculated from the modified VATM proposed in this study (“mod.VATM”) to account for the axial restraint provided by the axial stiffness of the longitudinal prestress reinforcement.

As referred in Section 1 of the article, VATM is able to predict the global behavior of RC beams under torsion throughout the entire loading history. However good results are observed only for high loading levels (Hsu and Mo 1995a, Bernardo *et al.* 2012a). This is because VATM assumes that the beam is extensively cracked from the beginning of the loading, which is not true. This explains the discrepancies observed between the experimental results and the analytical predictions from VATM and modified VATM for low loading levels in Fig. 8.

For Beam D2, neither the analytical predictions from VATM nor the same ones from the modified VATM approaches very well the experimental resistance torque. In its original study, Bernardo 2003 point out that, for some unknown reason, Beam D2 exhibit a somewhat excessive resistance torque, when compared with Beam D1. According to the author, the resistance torque of Beams D1 and D2 should be similar because, despite Beam D2 has slightly higher prestress force and higher prestress reinforcement area, Beam D2 has also smaller compressive concrete strength (see Table 2).

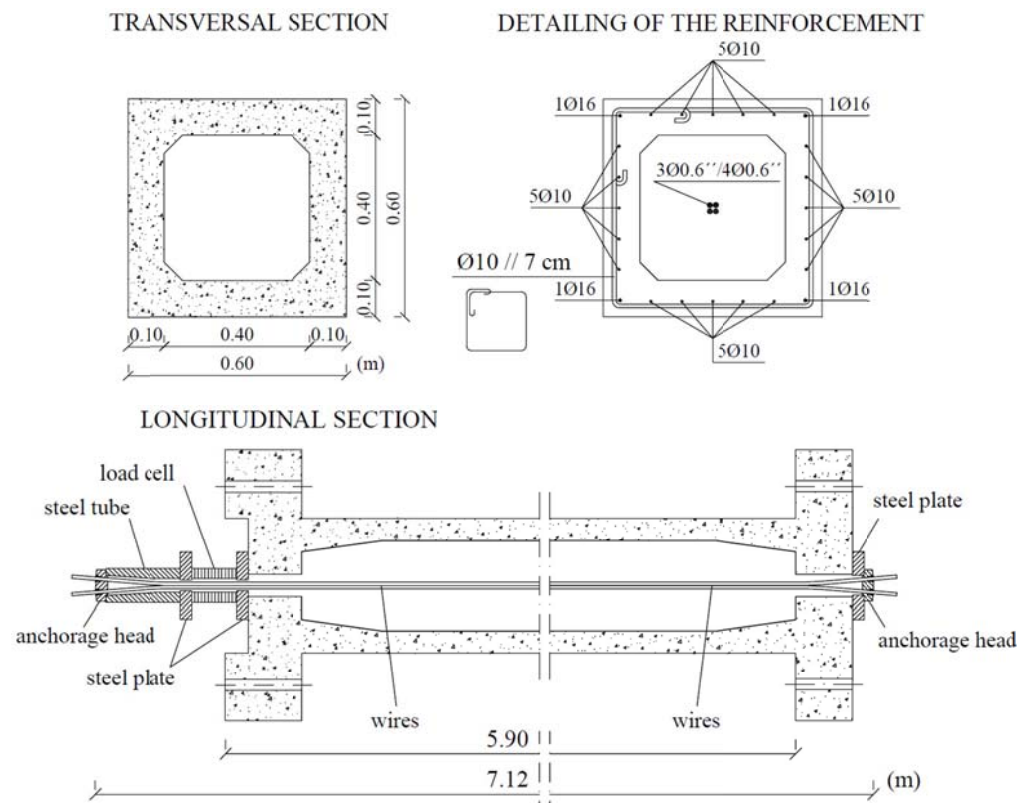


Fig. 7 Geometry and detailing of test Beams D1 and D2 (Bernardo 2003)

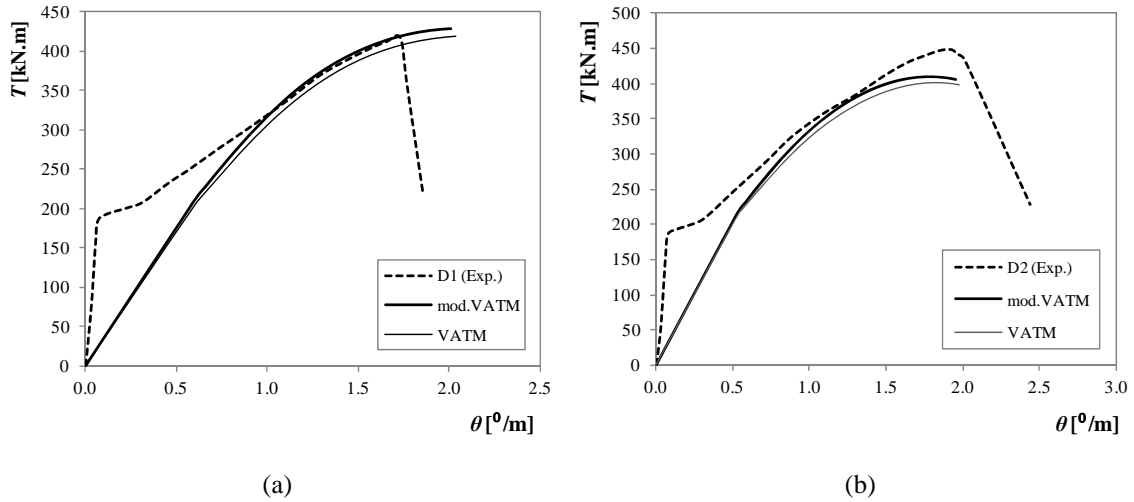

 Fig. 8 $T - \theta$ curves: (a) Beam D1 - (b) Beam D2

Table 2 Properties of experimental PC hollow beams D1 and D2 (Bernardo 2003)

Beam	$x; y$ cm	t cm	x_1 cm	y_1 cm	A_{st} cm ²	A_{st}/s cm ² /m	A_{pt} cm ²	ρ_l %	ρ_t %	f'_c MPa	f_{ly} MPa	f_{ty} MPa	$f_{p0,1\%}$ MPa	f_{pi} MPa	f_{ep} MPa	$E_c^{(1)}$	$\epsilon_o^{(1)}$ %	$\epsilon_{cu}^{(1)}$ %	k kN/m
D1	60	11.4	54.3	54.2	23.8	11.2	4.2	0.66	0.68	80.8	724	715	1670.5	640	1.79	41.2	0.21	0.30	11503
D2	60	11.5	55.5	55.5	23.8	11.2	5.6	0.66	0.69	58.8	724	715	1670.5	1100	3.08	37.4	0.20	0.35	15337

⁽¹⁾ Calculated from EC2 2010

Despite of the previously referred with respect to Beams D2, Fig. 8 shows that the modified VATM proposed in this study slightly improve the previsions of the $T - \theta$ curves for the ultimate behaviour of Beams D1 and D2, when compared with the same ones computed from VATM. The slight differences between the theoretical $T - \theta$ curves are probably due to the low level of axial restraint provided by the longitudinal prestress reinforcement. In fact, the reinforcement area (A_{pt}) is not very high. Nevertheless, some axial restraint effect exists and the theoretical $T - \theta$ curves from the modified VATM are closer to the experimental ones.

Since only two test beams were used to validate the modified VATM proposed in this study, the obtained results cannot be considered conclusive. For this reason, a comparative analysis with numerical results is presented in the next section.

5. Comparative analysis with FEM

In the present section, a comparative analysis will be carried out with the help of some numerical results from a three-dimensional nonlinear finite element analysis by using LUSAS software (LUSAS 2010). The comparative analysis will be focused on the ultimate behaviour, namely the torsional strength, of a RC hollow beam under torsion.

5.1 Experimental beam

For the purpose of the present section, the tested RC hollow beam A2 (or A-47.3-0.76) from Bernardo and Lopes (2009) will be simulated under torsion and until failure with different levels of axial restraint. Among all the tested beams from Bernardo and Lopes 2009, Beam A2 was the one with the highest torsional ductility, so it will be interesting to study also the influence of the axial restraint level on this important property. This beam was also chosen because hollow sections are a current solution when high torsional forces exist.

The geometry (similar to Beams D1 and D2, Fig. 7) and detailing of Beam A2 is presented in Fig. 9. The ordinary reinforcement used in Beam A2 (A500 Class) were ribbed bars (diameters of 8, 10 and 12 mm). Elastic modulus of the steel, E_s , was assumed to be 200 GPa. Table 3 summarizes the geometrical and mechanical properties of the experimental Beam A2. In Bernardo and Lopes (2009), Beam A2 was subjected to pure torsion until failure with no axial restraint.

5.2 Finite element model

The numerical model used in this study is a nonlinear tridimensional finite element model (3D FEM) developed with LUSAS software (LUSAS 2010). This numerical model aims to simulate the global behaviour of the RC Beam A2 under torsion and under several axial restraint levels. The experimental results of Beam A2 (without axial restraint) are used to validate the FEM. This latter consisted of thick steel plates in the tops of the beam (section under torsional loading and section with bearing supports), and RC walls composing the hollow section, as illustrated in Figs. 10 and 11.

The concrete walls and steel plates of the beam were modeled by eight-node solid elements with 3 degrees of freedom (translations) in each node (HX8 element, Fig. 12(a)). The steel reinforcement was modeled using a 3D isoparametric bar with two nodes and 3 degrees of freedom (translations) in each node (BRS2 element, Fig. 12(b)). HX8 and BRS2 are compatible with each other and also with nonlinear analysis. Perfect bond was considered between concrete and reinforcement bars (no slip exists), so solid and bar steel elements share the same nodes. The sizes of the mesh in the RC walls were conditioned by the small spacing between longitudinal and transversal bars (Fig. 10). The thick plates on top sections of the beam act as a force transfer element and were modeled with rigid HX8 elements and tied to the top sections of the beam. The model was subjected to a binary of imposed displacements in one of the top section in order to simulate the applied torque. The opposite top section was simply supported in several nodes in order to simulate a fully restrained twist condition (Fig. 10). Axial restraint was simulated with a longitudinal and external tie (steel cable modeled with BRS2 elements, Fig. 12(b)) linked to the steel plates at the top sections of the beam (Fig. 10). The transversal area of this element is variable, depending on the axial restraint level to be simulated. The FE model for Beam A2 add a total of 5540 nodes, 2978 bar elements and 4044 solid elements.

5.3 Material models

A plastic-damage-contact model, called Multi-Crack (LUSAS 2010), was used to model the concrete both in compression and tension. This distributed fracture model is based on the Craft model from Jefferson 2003 and uses planes of degradation that can undergo damage and separation but which can regain contact according to a contact state function. The model is able to

simulate the type of delayed aggregate interlock behaviour exhibited by fully open crack surfaces that subsequently undergo significant shear movement. To simulate the nonlinear behaviour for the concrete in compression the model has a fully integrated plasticity component that uses a smooth triaxial yield surface and frictional hardening-softening functions. For concrete in tension, a softening curve as shown in Fig. 13 is used. The loss of tensile strength is related with the degree of concrete crushing in compression. The model was validated with experimental data related to reinforced concrete under shear (Jefferson 2003), so it can be applied to elements under torsion. A more detailed characterization of the Craft model can be found in Jefferson 2003.

In addition to the uniaxial concrete compressive strength (f'_c) and concrete Young's Modulus (E_c) from Table 3, Table 4 presents the assumed values for the other several concrete properties parameters incorporated into the Multi-Crack model. For the strengths, average values were used. Since the cross section is hollow, the effect of confinement in concrete due to the transversal reinforcement was neglected.

For ordinary reinforcement, the average $\sigma - \varepsilon$ relationship from Belarbi and Hsu (1994) was used (Table 1). Figure 14 presents the $\sigma - \varepsilon$ relationship (continuous curves and simplified curves) for the longitudinal and transversal reinforcement. Such curves were computed from equations presented in Table 1, using steel properties presented in Table 3 and described in Section 5.1. Poisson's coefficient for the reinforcement was assumed to be 0.3.

For the external tie (steel cable) and thick plates, a linear $\sigma - \varepsilon$ relationship was assumed with no upper limit for stress. A Young's Modulus of 200 GPa was assumed for the external tie.

5.4 Convergence criteria and validation

For the nonlinear analysis, a solution procedure was adopted in which the total required load is applied in a number of automatic increments. In this study, the torsional load was simulated with a binary of imposed displacements (Fig. 10), so displacement incrementation was used. The starting load factor was assumed to be 1 mm and the maximum change in load factor was fixed to 2 mm. The incremental-iterative solution was based on modified Newton-Raphson iterations. In order to improve convergence characteristics, namely for high level loading, the constant load control method switched to arc-length method by imposing a stiffness ratio limit. Automatic increment reductions were also used when an increment fails to converge.

The convergence criterions used were the residual force norm, displacement norm and the external work norm. The solution termination was specified by limiting the maximum applied load factor. The chosen initial value was based on the maximum experimental twist observed for Beam A2.

In order to validate the numerical model, Fig. 15 presents the $T - \theta$ curves for Beam A2. Both experimental and numerical $T - \theta$ curves are presented. For each converged point, the numerical torsional moments and twists were computed from the reaction forces in the supports and from the imposed displacements at the top sections of the model (Fig. 10), respectively. Comparison between experimental and finite element analysis shows that, generally, good agreement exists until the maximum torque is reached. After this point, numerical convergence was difficult to achieve. So the maximum applied load factor was reduced in order to allow computing only the initial part of the descending branch of the $T - \theta$ curve (to be sure that maximum torque was reached).

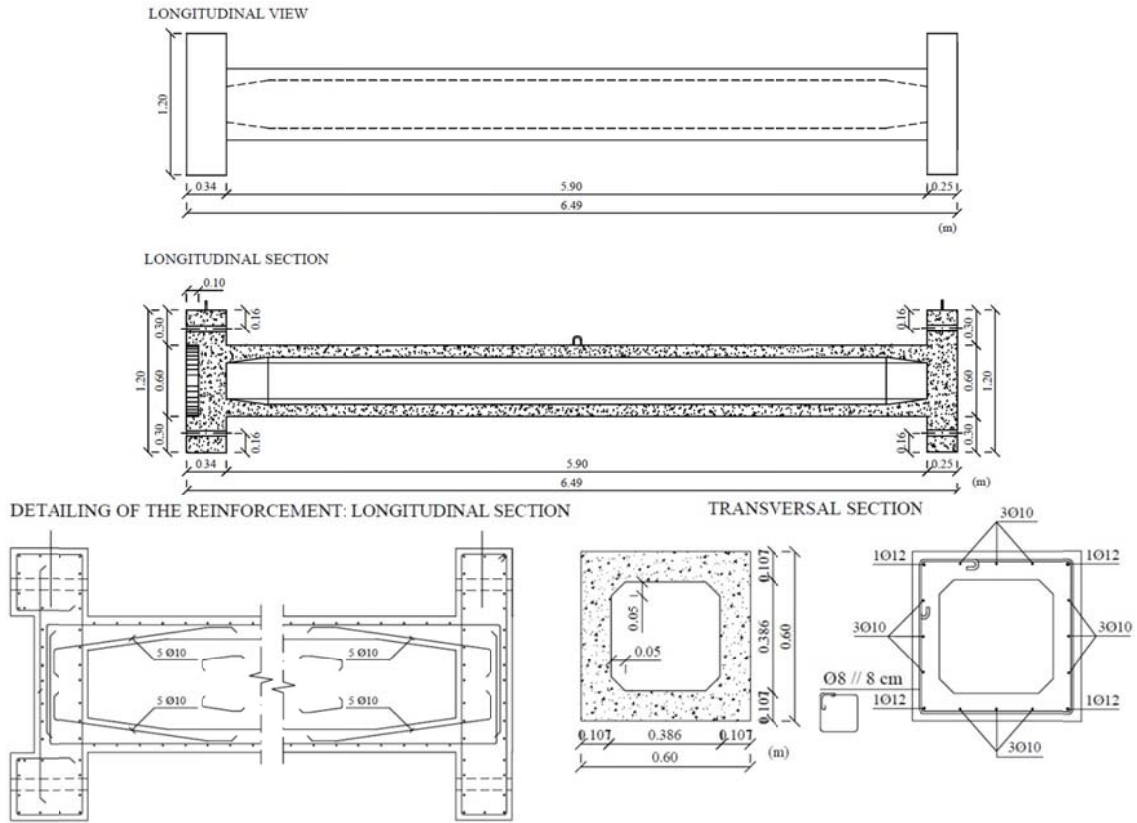


Fig. 9 Geometry and detailing of test Beam A2 (Bernardo and Lopes 2009)

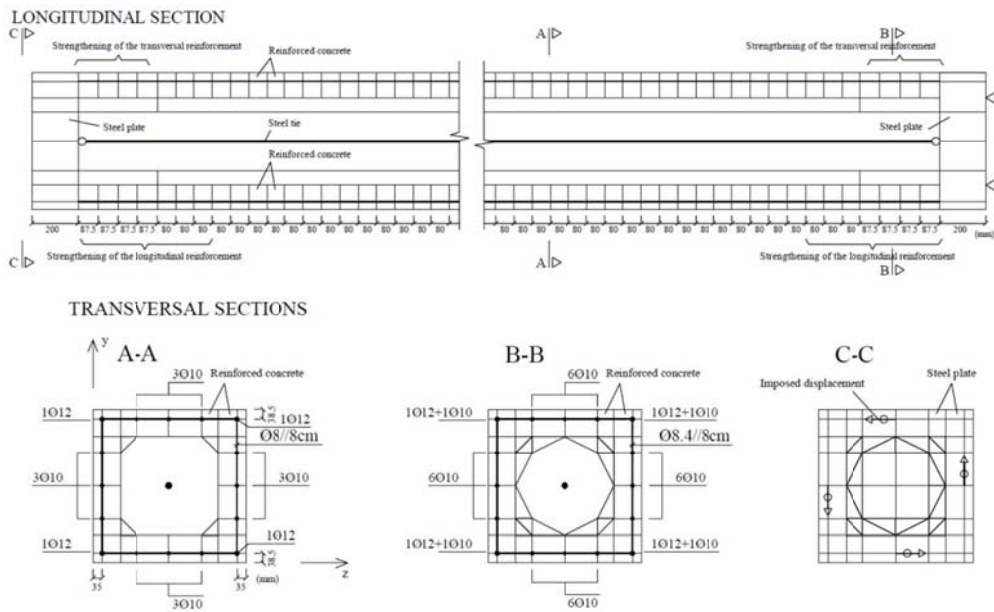


Fig. 10 3D FEM for Beam A2: Mesh

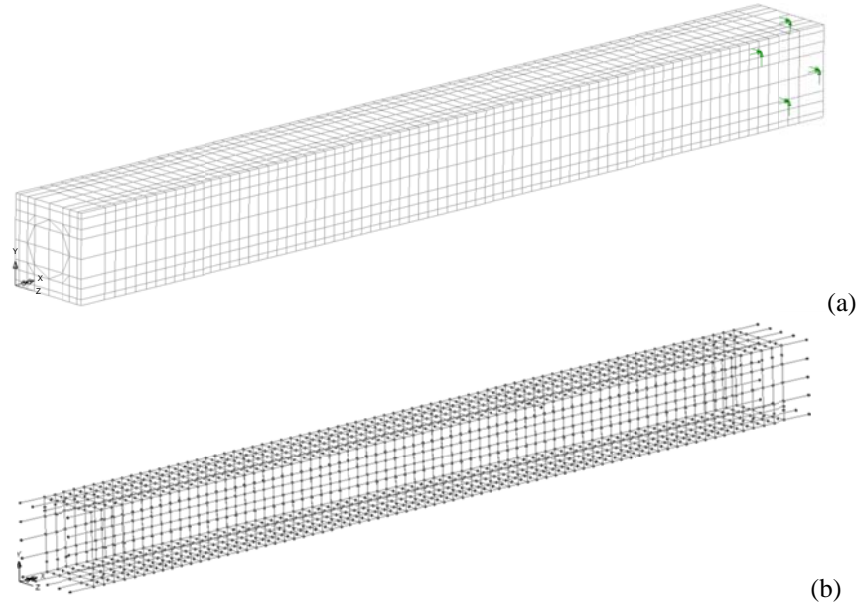


Fig. 11 3D FEM for Beam A2: (a) Concrete + Steel plates – (b) Reinforcement

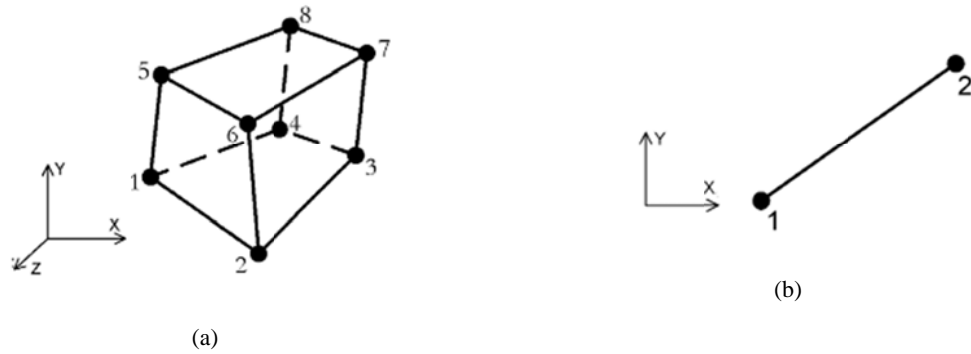


Fig. 12 Finite elements model: (a) 8-node element (HX8) – (b) 2-node element (BRS2) (LUSAS 2010)

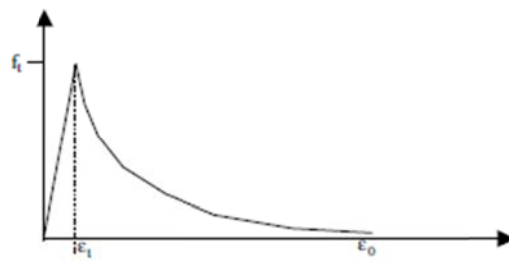
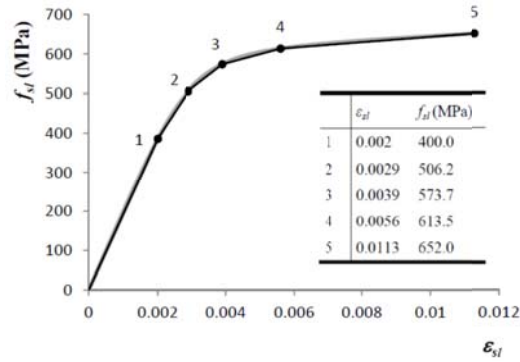
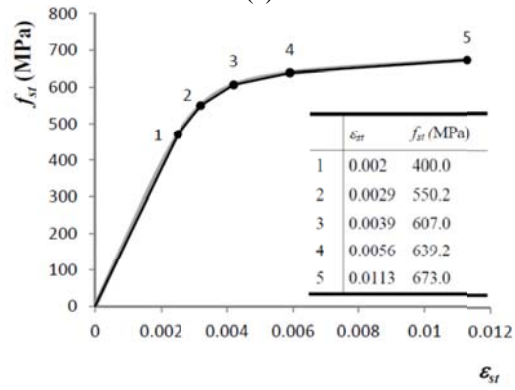


Fig. 13 Tensile softening curve (Jefferson 2003)



(a)



(b)

Fig. 14 Average $\sigma - \epsilon$ relationships: (a) longitudinal reinforcement – (b) transversal reinforcement

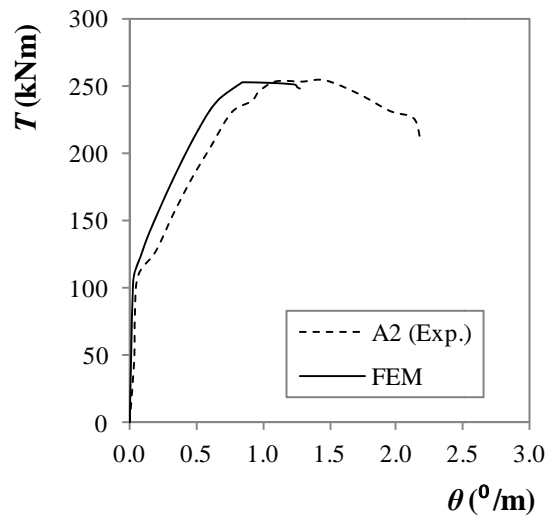


Fig. 15 $T - \theta$ curves for Beam A2

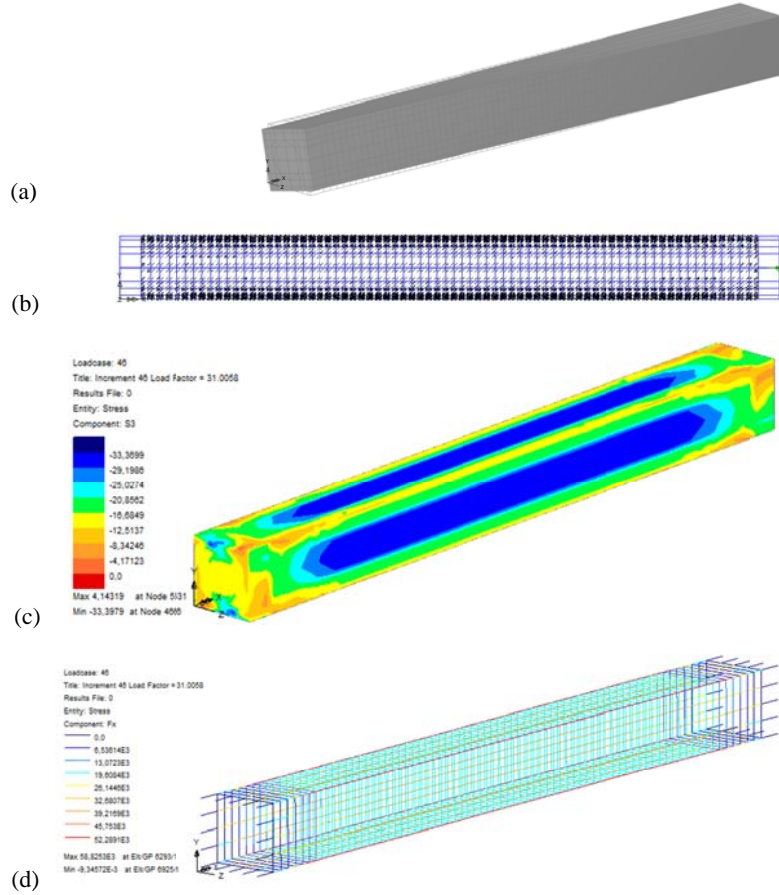


Fig. 16 FEM results: (a) deformation – (b) cracking – (c) principal compressive stress in concrete – (d) tensile stress in reinforcement

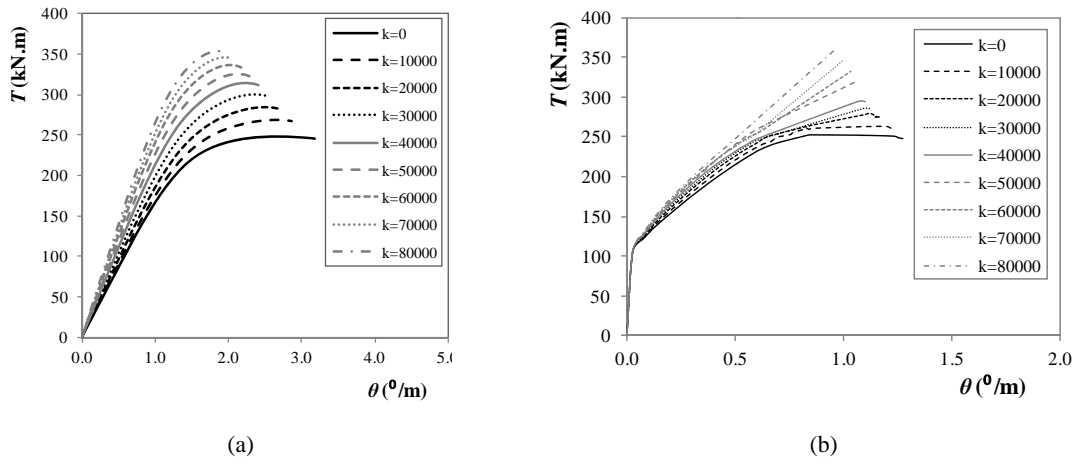


Fig. 17 $T-\theta$ curves for Beam A2: (a) modified VATM – (b) FEM

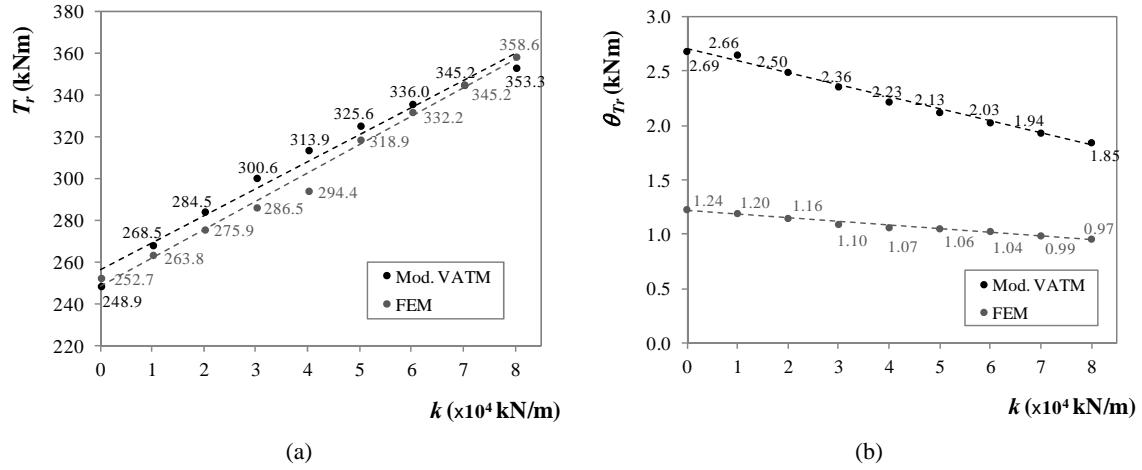


Fig. 18 Comparative analysis between modified VATM and FEM results

Table 3 Properties of experimental RC hollow beam A2 (Bernardo and Lopes 2009)

Beam	$x ; y$ cm	t cm	x_1 cm	y_1 cm	A_{st_2} cm ²	A_{st_2}/s cm ² /m	ρ_l %	ρ_t %	f'_c MPa	f_{ly} MPa	f_{ly} MPa	$E_c^{(1)}$	$\varepsilon_o^{(1)}$ %	$\varepsilon_{cu}^{(1)}$ %
A2	60	10.7	53.8	53.1	14.0	6.3	0.39	0.37	47.3	672	696	36.1	0.20	0.35

⁽¹⁾ Calculated from EC2 2010

Table 4 Concrete properties

Poisson's ratio - ν	0.2
Uniaxial tensile strength - f_t (MPa)	1.8 ⁽¹⁾
Strain at peak uniaxial compression - ε_c	0.002 ⁽²⁾
Strain at effective end of softening curve for distributed fracture - ε_o	0.07 ⁽³⁾
Fracture energy per unit area (for $\varepsilon_o > 0$) - G_f	0
Biaxial to uniaxial peak principal stress ratio - β_r	1.15
Initial relative position of yield surface - Z_o	0.6
Dilatancy factor giving plastic potential slope relative to that of yield surface - ψ	-0.1
Constant in interlock state function - m_g	0.425
Contact multiplier on ε_o for 1 st opening stage - m_{hi}	0.5
Final contact multiplier on ε_o - m_{ful}	10
Shear intercept to tensile strength ratio for local damage surface - r_σ	1.25
Slope of friction asymptote for local damage surface - μ	1
Angular limit between crack planes (Rad)	1

⁽¹⁾ Calibrated to adjust for the cracking torque

⁽²⁾ Calculated from EC2 2010

⁽³⁾ Calibrated to adjust for the maximum torque

Table 5 Axial stiffness values provided by the steel cable

Axial restraint level	A_p (cm ²)	k (kN/m)	Axial restraint level	A_p (cm ²)	k (kN/m)
1	0	0	6	14.75	50000
2	2.95	10000	7	17.70	60000
3	5.90	20000	8	20.65	70000
4	8.85	30000	9	23.60	80000
5	11.80	40000			

Fig. 15 shows that, along the twist axis, the “position” of the FEM T - θ curve between cracking torque and maximum torque does not match very well with the experimental T - θ curve, although the inclination (tangent torsional stiffness in cracked stage) is very similar. This is probably due to the high value considered for the strain $\varepsilon_o = 0.07$ at effective end of softening curve for concrete in tension (Table 4 and Fig. 13). As previously referred (note ⁽³⁾ in Table 4), this value was chosen in order to calibrate the model to adjust for the maximum torque. For lower values, it was observed that the FE program prematurely stopped the calculations because the final point of the softening curve for concrete in tension was reached. Since ε_o is relatively high, higher influence of the tensile concrete after cracking torque exists (as ε_o increases, the area of the softening curve illustrated in Fig. 13 between ε_r and ε_o also increases), so the secant torsional stiffness of the beam also increases.

From Fig. 15, it can be also observed that the descending branch of the FEM T - θ curve, after the maximum torque is reached, starts somewhat prematurely when compared with the experimental T - θ curve. Thus, the torsional plastic capacity (inelastic deformation) of Beam A2, after maximum torque is reached, is not perfectly foreseen by FEM. This is probably due to the assumed hypothesis that perfect bond exists between concrete and reinforcement bars, as previously explained in Section 5.2. It is known that in the inelastic stage, high slip can exist between bars and concrete, so the inelastic deformations would be higher.

Another reason for the discrepancies previously observed is also probably related to the fact that the eight noded solid elements (with 3 translational Degree of freedoms per node) used to model the concrete walls of the beams are usually associated with a problem of shear locking. Reduced integration or incompatible modes are generally used as remedy to overcome shear locking. In this study none of these methods has been adopted to overcome the problem of shear locking.

Since the comparative analysis in this section is mainly focused on the torsional strength, it is considered that the previously observed discrepancies in Fig. 15 are less important. This is because for design purpose of RC sections under torsion, the torsional strength is the most important parameter for safety. So, the FEM was accepted for the purpose of this study and no additional calibrations were performed.

Fig. 16 shows some numerical results from FEM, namely: the deformed mesh (Fig. 16(a)), the cracking pattern (Fig. 16(b)), the principal compressive stress in concrete (Fig. 16(c)) and the stress in the reinforcement for the maximum torque (Fig. 16(d)).

5.5 Comparative analysis

In this section, a comparative analysis focused on the ultimate behaviour of Beam A2 with several axial restraint levels will be carried out. The results from the FEM and the modified

VATM will be compared. Since the axial restraint in the FEM is simulated by incorporating an external steel cable (Fig. 10), as explained in Section 5.2, Table 5 resumes the range of values considered for the axial stiffness k provided by the steel cable and calculated from Eq. (43). The length l_p of the steel cable and the Young's Modulus of the material were fixed to constant values (5.90 m and 200 GPa, respectively), so only the area of the cross section (A_p) varied.

Fig. 17 presents the T - θ curves for Beam A2 with several axial restraint levels computed from the modified VATM (Fig. 17(a)) and from the FEM (Fig. 17(b)). The T - θ curves from the two models were not incorporated into one unique graph because they are relative to very different models for low level of loading. In fact, VATM consider the element fully cracked from the beginning of the loading, whereas FEM consider the participation of tensile concrete. So, torsional behaviour for low to medium level loading is very different for each model (see Fig. 17).

Fig. 17 seems to show that the last portion of the T - θ curves (ultimate behavioral part) from Modified VATM and FEM are in good agreement. It can be also state that the maximum torque and the torsional stiffness in cracked stage increase as the axial restraint level increases. However, it can be also state that the inelastic deformations decreases as the axial restraint level increases. Then, torsional failure becomes more fragile as the axial restraint level increases. This is due to the influence of the compressive longitudinal stress state in the concrete struts associated to the axial restraint.

Fig. 18(a) presents the evolution of the torsional strength (maximum torque, T_r) for the several axial restraint levels (k) considered in this study. Fig. 18(a) shows that modified VATM and FEM give very similar values for T_r (see values in graph). The observed tendency lines for T_r (linear regression) are also very similar. The maximum difference observed between T_r values from modified VATM and FEM is only 6.6%. So, it can be state that FEM validates the modified VATM in order to compute the torsional strength of axially restrained beams. It should be also noted that the increase in the torsional strength, as the axial restraint level increases, is notable. In average, for each increment of $k = 10000$ kN/m, torsional strength increases 4.5% (this value is the same for both models). This clearly shows the benefice in torsional strength due to axial restraint.

Despite the discrepancies previously observed for the twists in Fig. 15, Fig. 18(b) presents the evolution of the twists corresponding to torsional strength (θ_{T_r}). For FEM, the ultimate twist was taken as the maximum twist value before T - θ curves begins to fall. Fig. 18(b) shows that θ_{T_r} values from FEM are lower when compared with the same ones from Modified VATM. As previously explained, VATM assumes a fully cracked stage from the beginning of loading. Then, the corresponding twists for high level loading are generally overestimated when compared with other models incorporating the participation of tensile concrete. Another reason for the discrepancies observed and related with the low ultimate twist values obtained from FE analysis, when compared to analytical predictions, is probably related with the problem of shear locking previously referred in Section 5.4.

Despite of this, both models shows that the ultimate twist decreases as axial restraint level increases. This shows that some negative influence of axial restraint exists on ultimate deformation capacity. So, torsional ductility decreases as axial restraint level increases.

6. Conclusions

In the first part of this article, a new and simply computing procedure, based on a modification of the VATM, to predict the ultimate behaviour of axially restrained RC beams was presented. In the second part, the theoretical predictions from the proposed theoretical model were compared to some experimental results available in the literature and also with numerical results from a three-dimensional nonlinear finite element analysis.

From this study, the following conclusions can be drawn:

- The proposed model, called modified VATM, is able to predict the ultimate behaviour of axially restrained RC beams under torsion;
- When compared to some experimental results available in literature (PC hollow beams with external and centered longitudinal prestress reinforcement), it was shown that the proposed model (modified VATM) improves the previsions for the $T - \theta$ curves for high level of loading (ultimate behaviour), when compared with VATM (without axial restraint);
- When compared to some numerical results from nonlinear 3D FEM (RC hollow beam under several axial restraint levels), it was shown that the proposed model (modified VATM) gives reliable values for the torsional strength;
- From the two previous conclusions, it can state that the modified VATM can be used for torsional design and allows for optimized design;
- It was also shown that torsional strength and torsional stiffness at cracked stage increases as the axial restraint level increases, approximately with a linear variation. Such observation shows the benefice of the axial restraint in the torsional strength and in the torsional stiffness in cracked stage;
- Some negative influence of the axial restraint on the ultimate behaviour of beams under torsion was also observed. In fact, the ultimate deformation decreases as axial restraint level increases. This aspect can negatively influence the ductility of beams under torsion and, therefore, should be take into account in design procedures.

It should be noted that the main results of this study were obtained from analyses carried out using RC and PC hollow beams under torsion (with squared section) as study model. For plain sections, it is well known that the concrete core has no influence in the ultimate torsional behaviour of the beams (Hsu 1968) and also that VATM gives good previsions regardless of the section type (plain or hollow) (Hsu and Mo 1985a 1985b, Bernardo and Lopes 2009, Bernardo *et al.* 2012a). For rectangular sections, the height to width ratio, if within current range values, has no notable influence as variable study (Hsu 1968) and VATM still gives good predictions (Bernardo and Lopes 2009, Bernardo *et al.* 2012a). So, the results of this study can also be extended to plain sections and quadrangular sections with current height to width ratios.

Finally, it should be also referred that the results obtained in this study were based on comparative analyzes performed between theoretical results and experimental results of only two specimens, complemented with some numerical results from a three-dimensional nonlinear finite element analysis. Despite of this limitation, the results indicate that the proposed analytical method (modified VATM) for axially restrained RC beams seems to be reliable. However, new projects aiming to testing axially restrained RC beams under torsion would be very useful for further analyses.

References

- Andrade, A.M., Bernardo, L.F.A. and Lopes, S.M.R. (2011), "TORQUE_MTEAV: ComputingTool to Evaluate the Ultimate Behaviour of Reinforced and Prestressed Concrete Beams in Torsion", *Proceedings of the International Conference on Recent Advances in Nonlinear Models – Structural Concrete Applications (CoRAN 2011)*, Coimbra, Portugal, November.
- Bernardo, L.F.A. (2003), *Torsion in Reinforced High-Strength Concrete Hollow Beams.*, Ph.D. Thesis, University of Coimbra, Portugal. (in Portuguese)
- Bernardo, L.F.A. and Lopes, S.M.R. (2009), "Torsion in HSC hollow beams: strength and ductility analysis", *ACI Struct. J.*, **106**(1), 39-48.
- Bernardo, L.F.A., Andrade, J.M.A. and Lopes, S.M.R. (2012a), "Softened truss model for reinforced NSC and HSC beams under torsion: a comparative study", *Eng. Struct.*, **42**, 278-296.
- Bernardo, L.F.A., Andrade, J.M.A. and Lopes, S.M.R. (2012b), "Modified variable angle truss-model for torsion in reinforced concrete beams", *Mater. Struct.*, **45**(12), 1877-1902.
- Bernardo, L.F.A., Andrade, J.M.A., Nunes, N.C.G. (2014), "Generalized softened variable angle truss-model for reinforced concrete beams under torsion", *Mater. Struct.*, **48**(7), 2169-2193.
- Belarbi, A. and Hsu, T.C. (1991), "Constitutive laws of softened concrete in biaxial tension-compression", *Research Report UHCEE 91-2*, University of Houston, Houston, Texas.
- Belarbi, A. and Hsu T.C. (1994), "Constitutive laws of concrete in tension and reinforcing bars stiffened by concrete", *Struct. J. Am. Concrete. Ins.*, **91**(4), 465-474.
- Belarbi, A., Prakash S. and You, Y.M. (2009), "Effect of spiral reinforcement on flexural-shear-torsional seismic behavior of reinforced concrete circular bridge columns", *Struct. Eng. Mech.*, **33**(2), 137-158.
- CEB 1990, CEB-FIP MODEL CODE 1990, Comité Euro-International du Béton.
- CEB 1995, "Ultimate Limit State Design Models, A State-of-Art Report", *Bulletin d'Information N.º 223*, June.
- Cevik, A., Arslan, M.H. and Saracoglu, R. (2012), "Neuro-fuzzy modeling of torsional strength of RC beams", *Comput. Concr.*, **9**(6), 469-486.
- Comité Euro-International du Béton (CEB) (1990), *CEB-FIP MODEL CODE 1990*.
- Fib. 2010. Model Code 2010, First complete draft. Bulletin no 55.
- Hsu, T.T.C. (1968), "Torsion of structural concrete - behaviour of reinforced concrete rectangular members", *ACI Special Publication*, **18**, 261-306.
- Hsu, T.T.C. (1984), *Torsion of Reinforced Concrete*, Van Nostrand Reinhold Company.
- Hsu, T.T.C. and Mo, Y.L. (1985a), "Softening of concrete in torsional members-theory and tests", *ACI. J. Proc.*, **82**(3), 290-303.
- Hsu, T.T.C. and Mo, Y.L. (1985b), "Softening of concrete in torsional members - prestressed concrete", *ACI. J. Proc.*, **82**(5), 603-615.
- Hsu, T.T.C. and Zhu, R.R.H. (2002), "Softened Membrane for Reinforced Concrete Elements in Shear", *ACI Struct. J.*, **99**(4), 460-469.
- Hsu, T.T.C. and Zhang, L.X. (1997), "Nonlinear analysis of membrane elements by fixed-angle softened-truss model", *ACI Struct. J.*, **94**(5), 483-492.
- Jefferson, A.D. (2003), "Craft - a plastic damage - contact model for concrete. I. Model theory and thermodynamic considerations", *Int. J. Solids. Struct.*, **40**(22), 5973-5999.
- Jeng, C.H. and Hsu, T.T.C. (2009), "A softened membrane model for torsion in reinforced concrete members", *Eng. Struct.*, **31**(9), 1944-1954.
- Jeng, C.H., Chiu, H.J. and Chen, C.S. (2010), "Modelling the Initial Stresses in Prestressed Concrete Members under Torsion", *ASCE Conference Proceedings 369*, **162**, 1773-1781.
- Lou, T., Lopes, A. and Lopes, S. (2011), "Numerical Behaviour axially restricted RC beams", *Proceedings of the International Conference on Recent Advances in Nonlinear Models – Structural Concrete Applications*.
- LUSAS (2010), Lusas Finite Element System, version 14.3. FEA – Finite Element Analysis Ltd.

- Kingston-upon-Thames. England.
- NP EN 1992-1-1 (2010), *Eurocode 2: Design of Concrete Structures - Part 1: General Rules and Rules for Buildings*.
- Ramberg, W. and Osgood, W.R. (1943), Description of stress-strain curves by three parameters, *Technical Note No. 902*, National Advisory Committee For Aeronautics, Washington DC.
- Rausch, E. (1929), *Design of Reinforced Concrete in torsion*, Ph.D. Thesis, Berlin. (in German).
- Taborda, C.S.B. (2012), *The Effect of Axial Restraint on the Behaviour of RC Beams under Torsion*, Master Thesis, University of Beira Interior, Portugal. (in Portuguese).
- Valipour, H.R. and Foster, S.J. (2010), "Nonlinear analysis of 3D reinforced concrete frames: effect of section torsion on the global response", *Struct. Eng. Mech.*, **36**(4), 421-445.
- Waldren, P. (1988), "The significance of warping torsion in the design of straight concrete box girder bridges", *Can. J. Civil. Eng.*, **15**(5), 879-889
- Wang J. (2006), *Constitutive Relationships of Prestressed Concrete Membrane Elements*, Ph.D. Thesis, University of Houston, TX, USA.
- Zhang, L.X. and Hsu, T.T.C. (1998), "Behaviour and Analysis of 100 MPa Concrete Membrane Elements", *J. Struct. Eng. - ASCE.*, **124**(1), 24-34.

CC